# Variable fault tip propagation rates affected by near-surface lithology and implications for fault displacement hazard assessment.

**F.A. Livio[1], M.F. Ferrario[1], C. Frigerio[1], A. Zerboni[2], A.M. Michetti[1].**

[1] Università degli Studi dell'Insubria, Dipartimento di Scienza ed Alta Tecnologia, Via Valleggio, 11 – 22100 Como (Italy).

[2] Università degli Studi di Milano, Dipartimento di Scienze della Terra "A. Desio", Via Mangiagalli 34 – Milano (Italy).

Corresponding Author: Franz Livio (franz.livio@uninsubria.it )

**Abstract**

The fabric of reverse fault zones at surface is usually partitioned in between a narrow discrete rupture zone and a more distributed one, where folding is predominant. This makes quite challenging the adoption of proper setbacks in surface rupture hazard studies for critical facilities or microzoning. Some of the parameters controlling fault zone fabric are related to mechanics of near-surface geology, (lithology, overburden thickness, cohesion and water content) whose interaction is complex an only partially understood. Nevertheless, these can be hardly measured or derived. Kinematic models, conversely, express such an interaction of complex variables as simple synthetic parameters, such as the amount of upward propagation of the fault tip for unit of slip, usually referred to as the P/S ratio (Propagation on Slip). Here, we discuss results on the trishear kinematic inverse modelling of a decametric – scale, contractional fault propagation fold at Monte Netto Hill (Capriano del Colle, N. Italy), observing a two-stage fault and fold growth evolution, marked by a significant shift in the P/S parameter. At this site, exceptional sequence of exposures due to ca. 10 years of quarry excavations allowed to obtain a series of cross-sections across the fault zone. We use this detailed, high-resolution, example as a natural "analog" for more general, large-scale surface ruptures involving a thick alluvial cover, a very common setting for siting of critical facilities.

During the early stage of displacement, the fault cut through clast-supported fluvial gravels with a high propagation rate (P/S = 7) and a discrete rupture width. Then, during the latest movements of the thrust, fault tip propagation slowed down to P/S ≈ 2.9, as the fault started cutting through several stacked bodies of pedogenized aeolian silts and overbank deposits causing a pronounced folding of the layers over a wider deformation zone. These results strongly suggest that lithological changes in the underlying stratigraphy, common in an alluvial plain depositional setting, would significantly affect the potential for surface faulting across the same tectonic structure, with relevant implications in the fault displacement hazard assessment.

## 1. **Introduction**

Current models of Fault Displacement Hazard Assessment (FDHA; e.g., ANSI/ANS-2.30, 2015) consider the probability of ground rupture and the amount of expected average slip at surface as primarily controlled by the magnitude of the maximum expected earthquake. Nevertheless, surface faulting can result in a narrow and discrete rupture zone, rather than in a broader and more distributed one, where folding is predominant: the so-called fault-zone fabric (e.g., Teran et al., 2015). The mode of fault propagation toward the surface has been recently investigated through numerical and analogue approaches (Moss et al., 2013, 2018; Thebian et al., 2018) providing insights on some of the most important parameters affecting surface faulting. Some of these parameters that control fault zone fabric are related to the characteristics of near-surface geology (i.e., lithology, overburden thickness, and water content; see Teran et al., 2015 for a review). An appropriate weighting of these variables could significantly enhance the prediction power of the extant FDHA methods. Unfortunately, these values are rarely directly measured, especially in the subsurface, and are usually assumed or derived in modeling.

Kinematic models, conversely, express the complex interaction of so many variables as simple synthetic parameters, solely relying on geometric assumptions with the main advantage of not implying the characteristics of the faulted rocks/sediments as, conversely, continuum mechanics or numerical analysis do. In trishear modeling, for example, such a key parameter is the amount of upward propagation of the fault tip for unit of slip, usually referred to as the P/S ratio (Williams and Chapman, 1983). This is the most effective parameter in controlling the final geometry predicted by trishear modeling (Allmendinger and Shaw, 2000). A progressive section restoration, using trishear modeling, allows to inspect variations of P/S through time and, if applied to large scale and near-surface sectors, can potentially investigate the kinematics of propagating faults at shallow depths, an issue of primary interest for FDHA. Trishear modeling has been demonstrated to be scale-

60 invariant, being applied for diverse issues including large scale case studies: the analysis of shallow
61 portions of crustal structures (Champion et al., 2001; Gold et al., 2006, Leon et al., 2007) and the
62 restoration of paleoseismological trenches across emerging faults (Chen et al., 2007; Lin et al.,
63 2007).

64 Here, we show results on the trishear kinematic inverse modeling of a contractional fault-
65 propagation fold in the Italian Southern Alps (Monte Netto, Capriano del Colle, Northern Italy). At
66 this site ca. 10 years of quarry excavations, exposed a series of cross-sections across the fault zone,
67 that was finally recently exposed in its core sector whilst, previously, only fault-related folding was
68 documented and dated in outcrop (Livio et al., 2014, Zerboni et al., 2014). This structure represents
69 a well-documented case study of a break-through fault propagation fold, cutting through a thick
70 Neogene sedimentary cover. Thanks to kinematic modeling we are able to derive the propagation
71 history of this thrust at depth from the near surface deformation. We obtained a consistent
72 restoration of the structure only supposing a two-step deformation process, marked by a
73 considerable lowering of P/S values as the fault, propagating to the surface, cut through different
74 lithologies. Our case study is focused on the analysis of a break-through fault propagation fold, over
75 a time-window of ca. $10^5$ years.

## 2. Geological framework

The study area is located at the northern margin of the Po Plain foredeep, along an array of E-W trending thin-skinned blind thrusts belonging to the western sector of Southern Alps (Castellarin et al., 2006; Castellarin & Cantelli, 2000). Deformation mainly involves, at depth, a syntectonic sequence of terrigenous units (Gonfolite Lombarda Gr. – Oligo-Miocene). Thrusts ramp up from a decollement located at the top of the underlying carbonates (Fantoni et al., 2004), deforming the overlying bedrock and the younger foredeep infilling of the Po Plain basin into fault-related folds.

The analyzed section exposes a decametric – scale secondary S-verging thrust and related fold, structurally linked at depth to a N-verging backthrust (i.e., the Capriano del Colle Backthrust; after Livio et al. 2009; 2014; Figure 1). The analysis of industrial seismic reflection data on highlighted the presence of growth strata dated from the Pliocene to Middle Pleistocene (Carcano & Piccin, 2002) and allowed to constrain slip rates of the backthrust as slowing down from 2.5 mm/yr to 0.43 mm/yr since the Pliocene (Livio et al., 2009). Capriano del Colle backthrust is associated to an overlying fault-related anticline, ca. N110 striking, eroded at both sides and folding early Pleistocene floodplain deposits (dated by biostratigraphy to 0.89 Ma (Carcano & Piccin, 2002; Scardia, 2006). Younger channel-belt and overbank deposits onlap the fold at both sides with a growth-strata architecture; older channels facies are occasionally present at the core of the hill (Figure 1). The structural culmination of this anticline is marked by the presence of a small isolated hill (i.e., the Monte Netto Hill) standing ca. 30 m above the surrounding alluvial plain. The plain was mainly built by fluvioglacial meltwater channels during the Last Glacial Maximum (Marchetti, 1996) and is presently incised by local drainage systems. Loess strata, interlayered by paleosols, cover the units at the top of the hill (Zerboni et al., 2014), progressively leveling subtle topographic depressions, including those due to coseismic tectonic deformation. The Monte Netto hill lies in the epicentral area of the Christmas 1222, Brescia earthquake (Io = IX-X MCS), one of the largest

seismic events in Northern Italy and earthquake-triggered soft-sediment deformations affecting fluvial units were observed and described at this site (Livio et al., 2009).

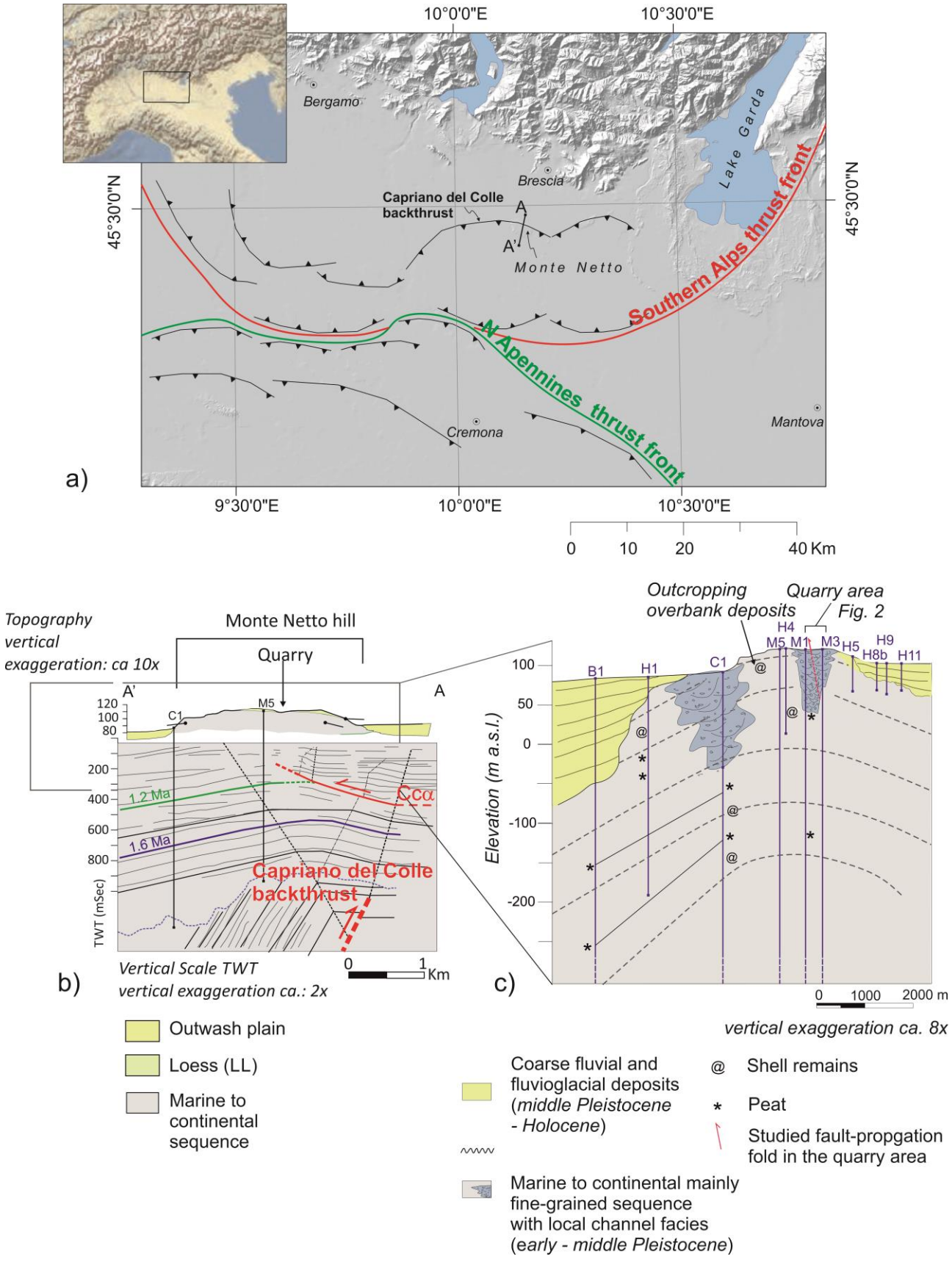


**Figure 1.** Geologic sections: a) structural setting; the study site is located on top of the Capriano del Colle backthrust, belonging to the Southern Alps buried thrusts belt; b) interpreted cross-section

106 across the Monte Netto Hill (modified after Livio et al., 2014); c) detailed geological cross-section
107 across the Monte Netto Hill highlighting lithological changes according to deep and shallow
108 borehole logs (see Figure S1 for borehole location and Logs).

109 A folded sequence of fluvial units and an onlapping loess-paleosols sequence is exposed in a quarry
110 area, located at the hilltop. The kinematic restoration of the outcropping anticline (Livio et al.,
111 2014), interpreted as a fault-propagation fold, indicated the presence of a ca. 24$^{o}$ dipping thrust
112 fault, with a tip line close to the surface (i.e., 10 m below the quarry floor) and a P/S value close to
113 3. It is noteworthy that these values resulted from the kinematic inverse modeling of the folded
114 sequence, but location of the fault tip was never observed in outcrop.

115 New excavations, performed in 2016, finally exposed the fault zone and offered the opportunity to
116 constrain at shallow levels the kinematic relationship between faulting and related folding.

117 The deformed sequence, as it outcrops in the new section, is composed by fluvial pre-growth strata
118 (PGS in Figure 2) and 5 stacked layers of syn-growth overbank and aeolian weathered deposits
119 (GS1 to 5; Figure 2). Correlations with dated units exposed in previously analyzed sections (Livio
120 et al., 2014) allowed to constraints the age of the deformed sequence to Early–Middle Pleistocene to
121 present (see Figure S2)

122 Stratigraphic logs of water wells and deep boreholes, together with previously exposed outcrops,
123 indicate that a ca. 50 m thick sequence of clast-supported channel-facies gravels (the lowermost unit
124 described by Livio et al., 2014; i.e., their FG08 unit) are lying ca. 5 m below the quarry floor. The
125 borehole locations and logs can be downloaded as Figure S1.

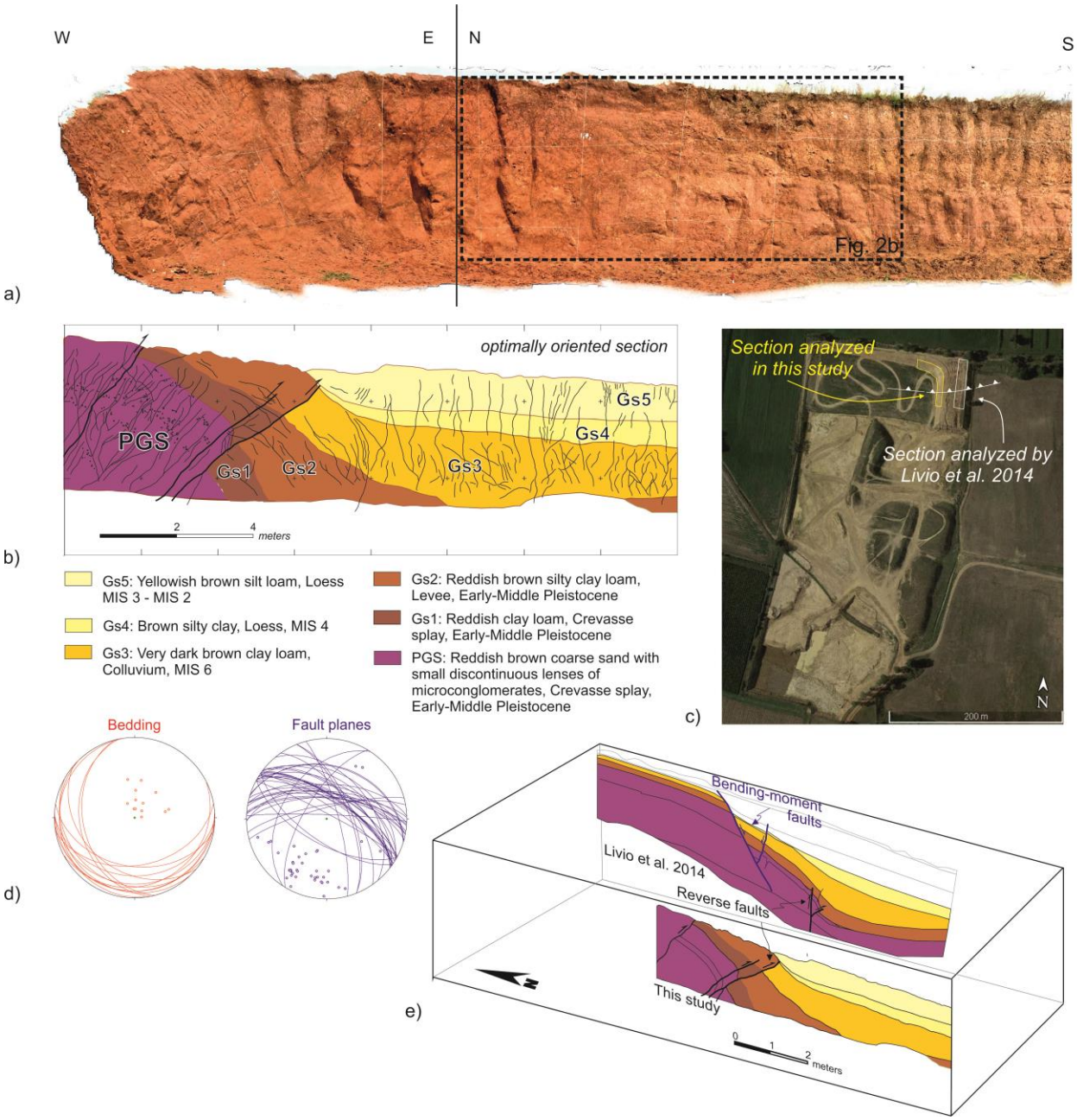


**Figure 2.** Field data from the outcropping sequence: a) ortho-photomosaic quarry wall exposed during the 2016 excavations (see Figure S3 for a full resolution version of the image), the outline of the logged section is indicated; b) section log: age constraints are derived from correlations with the units described by Zerboni et al. (2014); c) location of this section and of that one previously studied by Livio et al. (2014) (see Figure S2 for a comparison of the two logged sections); d) structural data: bedding and fault planes and poles, measured on the exposed section; e) comparison of the two sections in a 3D block-diagram.

## 3. Methods

We described the Monte Netto Hill section through a classical hand-drawing of a 1 m spaced grid logged at 1:10 scale and compared the geometries with a 3D model from a close-range photogrammetry (i.e., structure from motion) obtaining consistent results. For this purpose, we used a commercial version of the Agisoft Photoscan software. We then extracted an ortho-projection of the logged wall onto a plane trending normal to the fault strike. Final logging and restoration are based on this latter section. Structural data were acquired using the FieldMove Clino Android app, by Midland Valley, improving the productivity in field data acquisition; the same application allows collecting a great amount of statistically significant data.

We restored the section using a trishear numerical code (i.e., Fault Fold Code; Allmendinger, 1998; Zehnder & Allmendinger, 2000). This software performs a grid-search over the 6 parameters regulating trishear kinematic modeling (i.e., ramp angle, trishear angle, propagation on slip ratio, slip, X and Y of the fault tip position) attempting to restore to an original flat and horizontal geometry a reference horizon. The combination of best-fit parameters is that one minimizing the residual of the restored bed (i.e., chi-squared value). To minimize computing time, we performed our search in successive steps, firstly making evaluations over large regions of values and then focusing over smaller ranges, testing small increments in parameters value. Table 1 summarizes the parameters adopted during three successive steps of inverse grid search and best fit solutions, while statistics for all the tested models are reported in Dataset S3.

A detailed restoration of the section was then performed using the Move software by Midland Valley. We used a trishear 2D move-on-fault kinematic model to restore the section, assuming the best-fit parameters obtained by the grid-search analysis. Finally, we performed a step-by-step reconstruction of the fault and fold evolution with time, according to a fill-to-the-top architecture of syn-growth strata.

## 4. Results

Firstly, we performed a kinematic restoration of the top of PGS to a horizontal geometry. During grid search 1 (see Table 1), we tested all the six parameters, considering a range close to the observed one for ramp angle and final fault tip position. The best model correctly converges to the observed values and indicates a moderately narrow trishear angle ($20^o$) with a high P/S. Notably, best fitting displacement is the upper bound of the considered range, thus opening the possibility that more slip is needed to obtain best possible solutions.

Grid search 2 was then aimed at investigating higher displacements regions. Results indicate that a stable value of P/S is obtained also for a wide range of possible maximum slip on fault. Residuals are further decreasing as displacement increases, obtaining small increments in the model performance up to the upper bound of the displacement search window. We explored additional increments in slip on restoration, observing that further increments in slip resulted only in a slightly better linear fitting. Nevertheless, a contemporary progressive increase in the dip of the restored horizon appeared, leading to unlikely pre-growth geometries. We then constrained the most likely restoration to a pre-growth nearly horizontal geometry of PGS, by setting cumulative displacement to 13 m.

Table 1

*Grid searches with tested parameters (minimum, maximum, increment and the best fit value).*

| *Grid search* | *Tested models* | *Best fit chi square d* | *Ramp angle (R) - angle* | | *Trishear angle (T) - angle* | | *P/S* | | *Displacement (D) - cm* | | *Fault tip (x) - cm* | | *Fault tip (y) - cm* | |
|---|---|---|---|---|---|---|---|---|---|---|---|---|---|---|
| | | | *min-max (incr.)* | *Best fit* | *min-max (incr.)* | *Best fit* | *min-max (incr.)* | *Best fit* | *min-max (incr.)* | *Best fit* | *min-max (incr.)* | *Best fit* | *min-max (incr.)* | *Best fit* |
| **1** | 12375 | 29671 | 34 - 38 (1) | 35 | 10 - 90 (10) | 20 | 0 – 10 (1) | 8 | 0-1000 (20) | 1000 | 658-678 (5) | 658 | 430-450 (5) | 440 |
| **2** | 27225 | 23673 | 34 - 38 | 37 | 10 – 90 | 20 | 0 – 10 | 8 | 0-2000 | 2000 | 658- | 658 | 430- | 450 |

| | | | | | | | | | | | | | | |
|---|---|---|---|---|---|---|---|---|---|---|---|---|---|---|
| | | | (1) | | (10) | | (1) | | (50) | | 708 (5) | | 450 (5) | |
| **3** | 13650 | 7870 | - | 36 | - | 20 | 0 – 20 (1) | 7 | 0-1300 (2) | 1300 | - | 658 | - | 440 |

Finally, in grid search 3, we explored regions of higher P/S, since also values close to 10 (i.e., the upper bound range) were well performing in restoration during our first two attempts. Contemporary, we made the displacement to vary between 0 and 13 m. Figure 3b shows performance scores for the explored combinations of P/S and displacement in grid search 3. Our best-fit solution point to P/S = 7 with the smallest chi-squared for the maximum displacement allowed. Possible solutions with a lower slip (i.e., less than ca. 4 m) does not constraints P/S on a preferred value. Conversely, for larger displacement values, P/S close to 7 is the preferred solution, with smaller values unlikely.

Restoration of PGS to a sub-horizontal pre-growth geometry thus strongly suggests a relatively fast propagation of fault tip, in order to induce such a fault-propagation fold geometry. Nevertheless, such a solution does not appropriately restore the cutoffs of GS1 and GS2 layers since such a fast fault tip back-propagation with retrodeformation, still left some slip to be restored, as the fault tip has already migrated to deeper locations (Figure 3c). Preserved growth strata (i.e., GS1 and GS2) show a constant offset of ca. 1.6 meters, thus implying that strata deposition predated fault tip propagation across this sector. The offset of growth strata, across an along-fault distance of at least 4.65 m, indicates a maximum P/S ratio for this stage of deformation close to 2.9. We tried to apply such a solution for restoration but such low P/S values, on the other hand, does not unfold PGS accurately, resulting in un-acceptable geometries (Figure 3d).

We might therefore suppose a two-stage fault and fold growth evolution, marked by a significant shift in the P/S value parameter during growth. Firstly, fast fault propagation triggered the formation, at surface, of a wide fault propagation fold, and then, during the latest movements of the

thrust, the fault tip propagation slowed down to P/S ≈ 2.9. The latter resulted in marked asymmetric fold geometry, with a steep forelimb later faulted by the thrust itself (i.e., breakthrough thrusting). During these latest phases of deformation, several stacked bodies of aeolian sediments deposited, leveling the progressive structural relief cumulated by the thrust movements, and were cyclically weathered into a sequence of stacked paleosols.

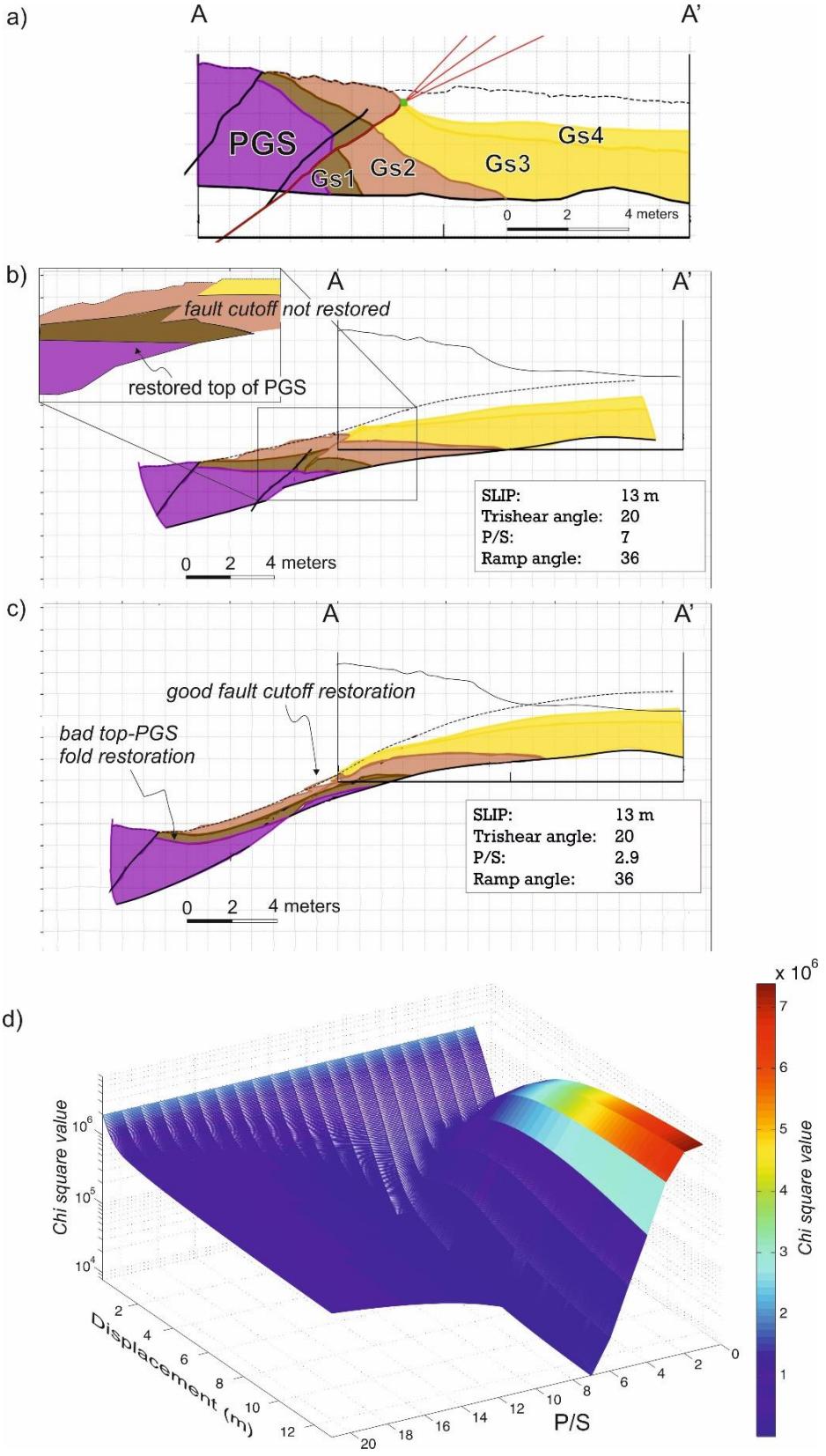


204

205 **Figure 3.** Schematic restoration through trishear kinematic modeling (see the text for further

206 details): a) deformed section to be restored, note the fault strand, in red, and the associated trishear

207 triangle at the fault tip; b) retrodeformation using the parameters obtained through the inverse grid

search approach: fault cutoff has not been properly restored; c) retrodeformation obtained using the P/S value measured at outcrop (i.e., 2.9): fold is not properly restored; d) chi-squared scores from grid search inversion n.3 (see Table 1) for variable P/S and displacement.

Finally, we performed a step-by-step restoration of the deformed sequence, considering constraints coming from kinematic modeling for fold restoration, field observations for cutoff retrodeformation, and progressive syn-growth sedimentation (Figure 4). We adopted straight fault line dipping 36°, lacking evidence for changes of dip with depth. Trishear angle is 20° and initial fault tip is assumed as derived from restoration analysis. Progressive fault slip is constrained by growth strata geometry, assuming that each sedimentation episode levels out any previous structural reliefs (i.e., fill-to-the-top approach) with a sub-horizontal top. P/S is set to 7 for almost the entire growth history, switching to 2.9 for the last step (i.e., step 5), as indicated by observations and discussion above.

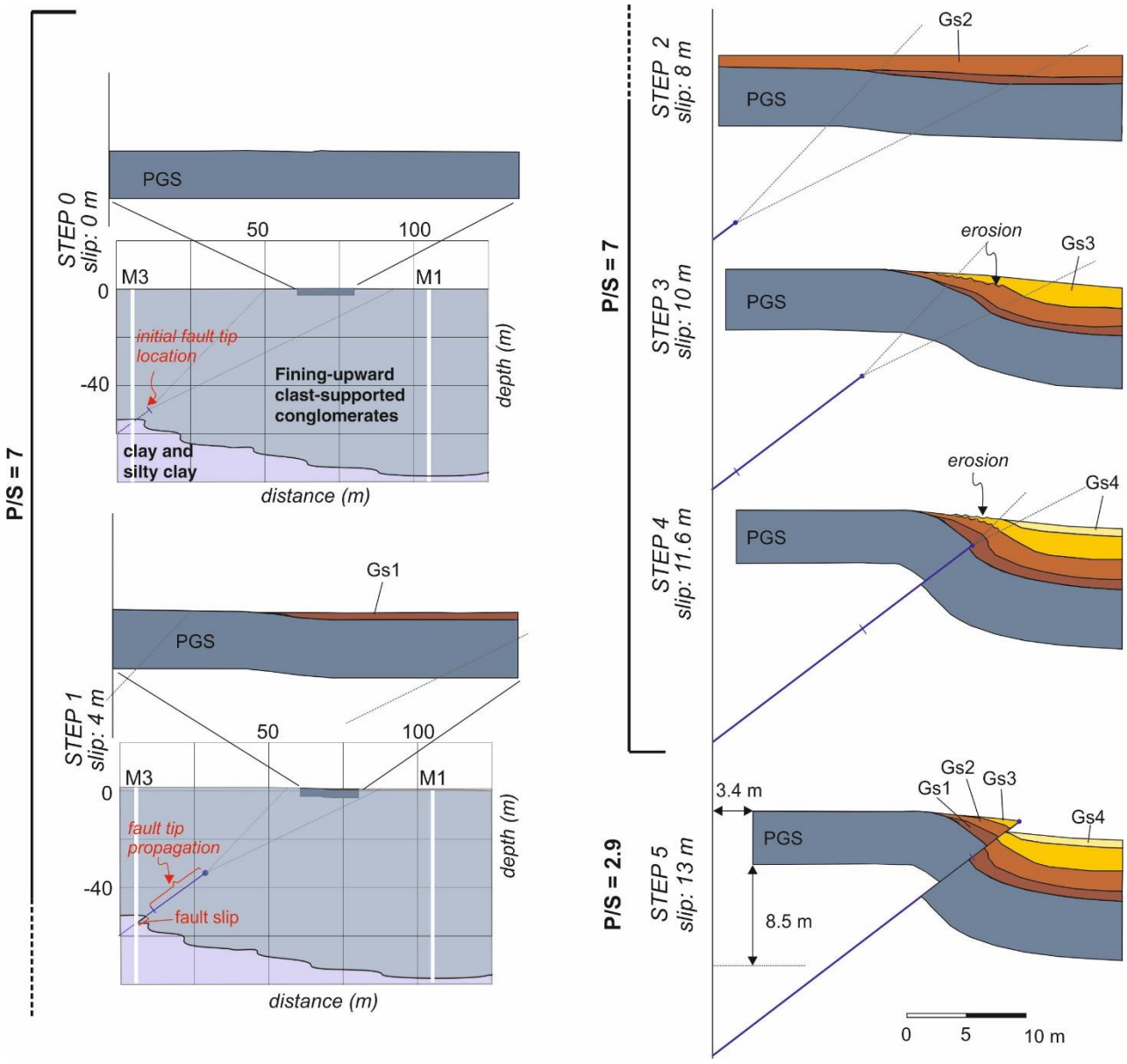


Figure 4. Forward modeling of the Monte Netto Hill thrust since Early-Middle Pleistocene to present adopting a variable P/S model: deeper stratigraphy in steps 0 and 1 is constrained by borehole logs (wells M1 and M3 as white lines; see also Figure S1).

These results are consistent with the stratigraphy of the hill beneath the site (Figure 1c and Figure 4), as observed in outcrops and reconstructed basing on borehole logs (see Figure S1). Here, from the top, the loess-paleosols sequence unconformably lies over ca. 5-10 meters of weathered overbank and colluvial deposits followed, downward, by a ca. 50 m thick sequence of channel-facies clast-supported gravels in a sandy matrix. It is noteworthy that, as the fault tip approaches the surface, we record a high P/S for the entire thickness of the clast-supported conglomerates, while the shifting to lower values corresponds to the crosscutting of fine-grained overbank, colluvial and

aeolian deposits. Also, the initial fault tip position (step 0 in Figure 4), as constrained by trishear restoration, lies close to the bottom of a level of clast-supported conglomerates unconformably overlying fine-grained overbank deposits. Likely, this latter lithologic discontinuity promoted the development of a ramp in the thrust.

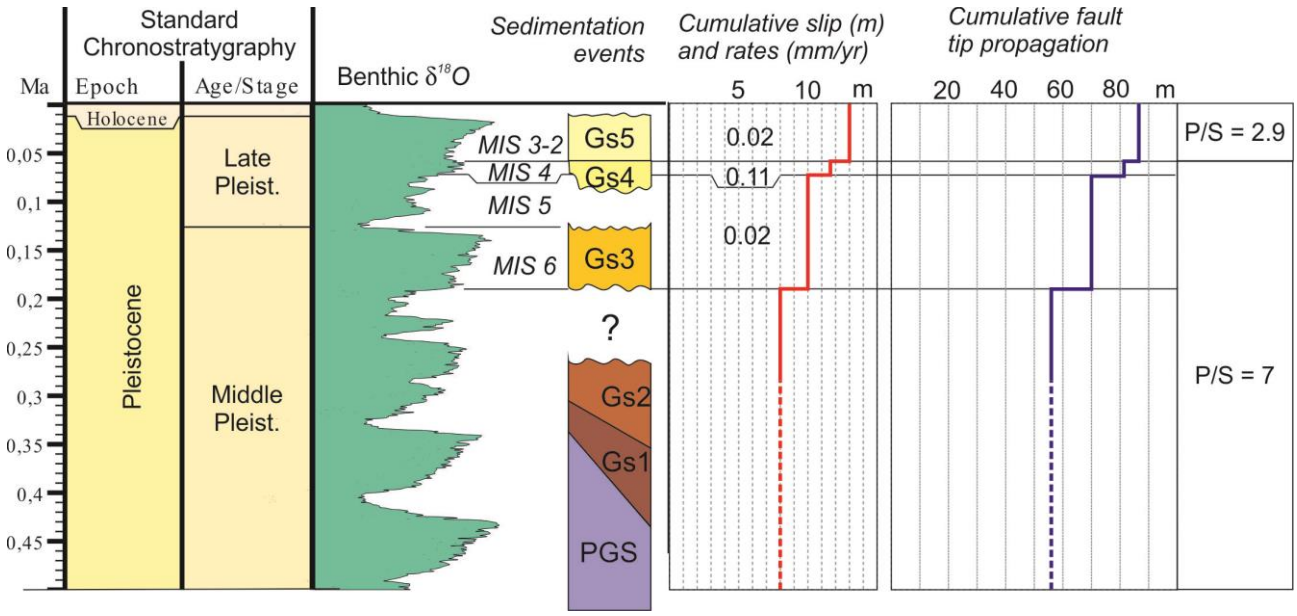


**Figure 5.** Cumulative slip and propagation of the fault tip as constrained by dated deposits: rates are also reported for every time window but the oldest one whose lower age constraint is lacking (dashed lines).

If we consider the temporal evolution of cumulative slip and fault tip propagation (Figure 5), as constrained by the age of the growth strata (i.e., Gs1 to Gs5), we observe that slip rates show limited changes through time except for the time window represented by Gs4, when we record 0.11 mm/yr. Such a high value could be an artifact due to a disconformity at the base of Gs4, and as suggested by the fact that the overall slip rate since Gs3 to present can be calculated in ca. 0.03 mm/yr, consistently with previous calculations by Livio et al. (2014). No considerable lowering of slip rates is recorded over a time window of $10^5$ yrs., thus confirming that the latest switch of

248 system to a slow propagating kinematic, is not partially due to a sensible decrease of deformation
249 rates.

## 5. Discussion: the influence of lithology on fault propagation

The kinematic restoration of the analyzed fault-propagation fold indicates that a single solution for structure retrodeformation is unsatisfactory, either for cutoff restoration or for unfolding. We thus assumed that upward fault tip propagation rate experienced a significant shift: the proposed two-stage model fits well with the stratigraphy, implying that this behavior is strictly dependent on the geo-mechanical properties of the cut lithologies and on the underlying stratigraphy. The temporal analysis of fault growth history (Figure 5) reveals that fault propagation rates are not correlated with the slip rates neither with the overburden through time. As discussed in Livio et al. (2014), in fact, the Monte Netto Hill started emerging from the surrounding plain around Marine Isotope Stage 6 (MIS 6; ca. 191-125 Kya), locally resulting in lack of sedimentation, only limited to intermittent aeolian deposition, and soil development. The zeroing of local accumulation rates, should have conversely resulted in an increased P/S ratio, as observed in analogue and numerical models (e.g., Lin et al., 2006): we argue that the vertical lithological discontinuities are the main drivers in determining the observed and modeled changes of fault propagation rates. Lithological discontinuities include here changes in the grain-size distribution of particles as well as weathering and soil development.

Mechanical properties of the ruptured materials strongly influence strain localization and amount of slip at surface, as observed following large earthquakes (Tchalenko & Ambraseys, 1970; Irvine & Hill, 1993; Lazarte et al., 1994; Johnson et al., 1997; Bray & Kelson, 2006; Fletcher et al., 2014; Teran et al., 2015; Floyd et al., 2016; Livio et al., 2016) or resulting from numerical and analogue modeling (Cole & Lade, 1984; Bray et al., 1994; Johnson & Johnson, 2002a; Cardozo et al., 2003; Moss et al., 2018). In particular, fault propagation rate is dependent on axial strain failure of soils (Bray et al., 1994), Young's modulus and dilation angle (Lin et al., 2006) or on viscosity coefficient, if material is approximated according to a viscous folding theory (Johnson & Johnson, 2002a). Overburden thickness, as well, strongly influences fault zone width and fabric at surface, resulting in different amount of slip on single fault strands (Tchalenko, 1970; Horsfield, 1977; Bray

et al., 1994; Schlische et al., 2002; Quigley et al., 2012; Zinke et al., 2014; Teran et al., 2015; Floyd et al., 2016). For a recent review of the literature on this issue the reader is referred Moss et al. (2018).

Our results, derived from a purely kinematic approach, confirm that: i) if geologically constrained, trishear kinematic models can be considered good analogues for mechanical models, with the advantage of being independent from geotechnical parameters (e.g., Cardozo et al., 2003); ii) P/S is the most affecting parameter, driving the output of a trishear model (Allmendinger and Shaw, 2000), which can be considered as the resultant of a combination of several mechanical and geotechnical characteristics of the cut lithologies (i.e., cohesion, water content, grain-size distribution etc.). The P/S values measured on several analogue models and using loose to dense sand, range from 5 to 50 (Cole & Lade, 1984; Bray et al., 1994; Anastosopoulos et al., 2007; Bransby et al., 2008; Moss et al., 2018), thus suggesting that these experimental materials are not perfectly scaled for large scale experiments of a near surface faulting prototype. Finite element modeling of reverse faulting through loose to stiff soils (Moss et al. 2018), obtained P/S values between 0.4 and 2. Recently, also Moss et al. (2013) came to a similar result, considering a geophysically-derived parameter for soil shear stiffness, as a synthetic descriptor for these characteristics. They made use of binomial regressions on a database of surface ruptures and found that the $Vs_{30}$ shear wave velocity was the best predictor for the tendency of faults to propagate through a medium, at least for reverse faulting. An additional considerable advantage of the kinematic approach is that a single parameter, resuming the rheological behavior of deformed material, can be easily incorporated into restoration process through a grid-search approach, thus minimizing the number of assumed parameters.

Our case study highlights a strong correlation of P/S with stratigraphy and with vertical lithologic changes. Thebian et al. (2018) discussed a similar dependency in the case of mechanical numerical modeling of fault propagation folds through soils: the adoption of depth-dependent soil parameters

301 is necessary for the correct simulation of natural analogues. Similarly, numerical models
302 investigating the enucleation and propagation of restricted faults through a multi-layered bedrock
303 (e.g., Roering et al., 1997; Roche et al., 2013) identified some medium-dependent parameters for
304 predicting the fault tendency to propagate (i.e., stiffness and strength contrasts) apart from strictly
305 deformation characteristics (i.e., amount of flexural slip and fault aspect ratio). Trishear numerical
306 modeling, if correctly set in the P/S and trishear angle parameters, well resembles results from more
307 complex mechanical approaches as those described above, and over a wide range of scales. In fact,
308 similar geometries are usually observed in outcropping examples or, at crustal scale, in thin-skinned
309 tectonics. Nevertheless, several examples are reported also for basement-involved thick-skinned
310 contractional tectonics (e.g., Horsfield, 1977; Chester et al., 1991; Narr & Suppe, 1994; Mitra &
311 Mount, 1998; Johnson & Johnson, 2002b), where upward fault propagation from basement to cover
312 is inhibited by the strong rheological contrast of the two crustal levels and typically results in drape-
313 folding and distributed deformation.

## 6. Conclusions

In this study, we performed the numerical restoration of a break-through fault-propagation fold using a trishear kinematic model. Our results point out the following major conclusions:

- solution derived from kinematic restoration must be carefully checked in their geological likelihood. As already pointed out by Allmendinger & Shaw (2000), trishear inverse modeling does not provide unique solutions and the possibility that best-fit solution does not correspond to a geologically sounding restoration, should be considered;

- our results indicate a two-stage fault deformation history, with a significant shift in the value of P/S parameter. The assumption that faults evolve with constant kinematic parameters can be an oversimplification of natural behavior;

- in our case study, (litho-)stratigraphy plays a significant role in determining P/S value changes with coarse and clast-supported channel-facies sediments promoting a fast fault tip propagation to the surface;

- the deduced lithological control on fault tip propagation velocity has significant consequences on the FDHA, implying a potential differential hazard for adjacent areas, depending on the underlying stratigraphy, rather than solely on fault parameters.

As for FDHA, we underline that these results imply that (litho-)stratigraphy should be considered in hazard assessment procedures both as lithological changes in the vertical column and as lateral changes, implying, in the latter case, a spatial dependency of ground break probability. The assessment of potential for surface faulting is gaining increasing interest for society, due to recent strong earthquakes that caused widespread and well-documented primary and secondary ruptures of ground surface (the 2010 Mw 7.2 Baja California eq., the 2010 Mw 7.1 Darfield and the 2016 Mw 7.8 Kaikoura earthquakes in New Zealand, the 2014 Mw 6 South Napa eq., the 2016 Mw 7 Kumamoto earthquakes in Japan; and the 2016 Mw 5.9 - 6.6 Central Italy earthquake sequence are

clear examples (Elliott et al., 2012; Fletcher & Spelz, 2009; Floyd et al., 2016; Hamling et al., 2017; Livio et al., 2016; Pucci et al., 2017; Quigley et al., 2016; Shirahama et al., 2016). Probabilistic FDHA is considered both in microzonation regulations, that recently included in Italy the mapping of capable faults (e.g. SM Working Group, 2015; Technical Commission for Seismic Microzonation, 2015) and for the siting of high-risk plants.

Moreover, these results have significant implications also for the assessment of the epistemic uncertainty in paleoseismological investigations. Since the latter is mainly based on the analysis of the on-fault effects and displacement at surface and considering that slow propagating faults can preferably accommodate deformation at surface as broad folding rather than discrete faulting, it is implicitly possible that some paleoevents could be missed, if a careful analysis of horizon's geometry is lacking during paleoseismological trenching. It is therefore recommended that an integrated approach must be provided, including high-resolution topographic surveys, nowadays easily available and cost-effective, such as, terrestrial and airborne LiDAR, close-range photogrammetry, total station topographic data.

Finally, the recognition of a P/S variable fault history opens the possibility that future kinematic models, integrating an inverse grid search approach, would make use of variable fault parameters with deformation, to optimize restoration processes.

**Acknowledgement**

We thank the municipality of Capriano del Colle, Brescia Province administration, and Fornaci Laterizi Danesi S.p.A. for permission to site access and trenching. An Academic License of MOVE® suite software was provided by Midland Valley and was used for fault/fold restoration.

## References

Allmendinger, R. W., 1998. Inverse and forward numerical modeling of trishear fault-propagation folds. Tectonics, 17(4), 640-656.

Anastasopoulos, I., Gazetas, G., Bransby, M., Davies, M., El Nahas, A., 2007. Fault rupture propagation through sand: Finite-element analysis and validation through centrifuge experiments. J. Geotech. Geoenviron. Eng. 133(8), 943–958.

ANSI/ANS-2.30, 2015. Criteria for Assessing Tectonic Surface Fault Rupture and Deformation at Nuclear Facilities. Published by the American Nuclear Society.

Bransby, M. F., Davies, M. C. R., El Nahas A., Nagaoka, S., 2008. Centrifuge modeling of reverse fault-foundation interaction. Bull. Earthq. Eng. 6(4), 607–628.

Bray, J. D., Seed, R. B., Cluff, L. S., Seed, H. B., 1994. Earthquake fault rupture propagation through soil. Journal of Geotechnical Engineering, v. 120, p. 543–561, doi:10.1061/(ASCE)0733 - 9410 (1994)120:3(543).

Bray, J. D., Kelson, K. I., 2006. Observations of surface fault rupture from the 1906 earthquake in the context of current practice. Earthquake Spectra, 22(S2), 69-89.

Carcano, C., Piccin, A., 2002. Geologia Degli Acquiferi Padani della Regione Lombardia. SELCA, Firenze.

Cardozo, N., Bhalla, K., Zehnder, A. T., Allmendinger, R. W., 2003. Mechanical models of fault propagation folds and comparison to the trishear kinematic model. Journal of Structural Geology, 25(1), 1-18.

379 Castellarin, A., Cantelli, L., 2000. Neo-Alpine evolution of the Southern Eastern Alps. Journal of
380 Geodynamics, 30, 251–274.

381 Castellarin, A., Vai, G., Cantelli, L., 2006. The Alpine evolution of the Southern Alps around the
382 Giudicarie faults: A Late Cretaceous to early Eocene transfer zone. Tectonophysics, 414, 203–223.

383 Champion, J., Mueller, K., Tate, A., Guccione, M., 2001. Geometry, numerical models and revised
384 slip rate for the Reelfoot fault and trishear fault-propagation fold, New Madrid seismic zone.
385 Engineering Geology, 62(1-3), 31-49.

386 Chen, W. S., Lee, K. J., Lee, L. S., Streig, A. R., Rubin, C. M., Chen, Y. G., Yang, H. C., Chang, H.
387 C., Lin, C. W. (2007). Paleoseismic evidence for coseismic growth-fold in the 1999 Chichi
388 earthquake and earlier earthquakes, central Taiwan. Journal of Asian Earth Sciences, 31(3), 204-
389 213.

390 Chester, J. S., Logan, J. M., Spang, J. H., 1991. Influence of layering and boundary conditions of
391 fault-bend and fault-propagation folding. Geological Society of America Bulletin, 103, 1059-1072.

392 Cole Jr., D. A., Lade, P. V., 1984. Influence zones in alluvium over dip-slip faults. Journal of
393 Geotechnical Engineering, 110(5), 599-615.

394 Collins, T. K., 1990. New faulting and the attenuation of fault displacement. Bulletin of the
395 Association of Engineering Geologists, 27(1), 11-22.

396 Elliott, J. R., Nissen, E. K., England, P. C., Jackson, J. A., Lamb, S., Li, Z., Oehlers, M., Parsons,
397 B., 2012. Slip in the 2010–2011 Canterbury earthquakes, New Zealand. J. of Geoph. Res.: Solid
398 Earth, 117(B3).

399 Fantoni, R., Bersezio, R., Forcella, F., 2004. Alpine structure and deformation chronology at the
400 Southern Alps-Po Plain border in Lombardy. Boll. Soc. Geol. Ital., 123(3), 463–476.

401 Ferrario, M. F., Livio, F., 2018. Characterizing the distributed faulting during the 30 October 2016,
402 Central Italy earthquake: A reference for fault displacement hazard assessment. Tectonics, 37.
403 https://doi.org/10.1029/2017TC004935.

404 Fletcher, J. M., Spelz, R. M., 2009. Patterns of Quaternary deformation and rupture propagation
405 associated with an active low-angle normal fault, Laguna Salada, Mexico: Evidence of a rolling
406 hinge? Geosphere, v. 5, p. 385–407, doi:10.1130/GES00206.1.

407 Fletcher, J. M., Teran, O. J., Rockwell, T. K., Oskin, M. E., Hudnut K. W., Mueller K. J., Spelz, R.
408 M., Akciz, S. O., Masana, E., Faneros, G., Fielding, E. J., Leprince, S., Morelan, A. E., Stock, J.,
409 Lynch, D. K., Elliott, J., Gold, P., Liu-zeng, J., Gonzalez-Ortega, A., Hinojosa-Corona, A.,
410 Gonzalez-Garcia, J., 2014. Assembly of a large earthquake from a complex fault system: Surface
411 rupture kinematics of the April 4, 2010 El Mayor–Cucapah Mw7.2 earthquake. Geosphere, 10,
412 797–827, doi:10.1130/GES00933.1.

413 Floyd, M., Walters, R., Elliot, J., Funning, G., Svarc, J. L., Murray, J. R., Hooper, A, J., Larsen, Y.,
414 Marinkovic, P., Burgmann, R., Johanson, I. A., Wright, T. J., 2016. Spatial variations in fault
415 friction related to lithology from rupture and afterslip of the 2014 South Napa, California,
416 earthquake. Geop Res Lett, 43(13), 6808-6816.

417 Gold, R. D., Cowgill, E., Wang, X. F., Chen, X. H., 2006. Application of trishear fault-propagation
418 folding to active reverse faults: examples from the Dalong Fault, Gansu Province, NW China.
419 Journal of Structural Geology, 28(2), 200-219.

420 Hamling, I. J., Hreinsdóttir, S., Clark, K., Elliott, J., Liang, C., Fielding, E., Litchfield, N, Villamor,
421 P., Wallace, L., Wright, T.J., D'Anastasio, E., Bannister, S., Burbidge, D., Denys, P., Gentle, P.,
422 Howarth, J., Mueller, C., Palmer, N., Pearson, C., Power, W., Barnes, P., Barrell, D.J., Van Dissen,
423 R., Langridge, R., Little, T., Nicol, A., Pettinga, J., Rowland, J., Stirling, M., 2017. Complex
424 multifault rupture during the 2016 Mw 7.8 Kaikōura earthquake, New Zealand. Science, 356(6334),
425 eaam7194.

426 Horsfield, W.T., 1977. An experimental approach to basement-controlled faulting. Geologie en
427 Mijnbouw, 56, 363–370.

428 Irvine, P. J., Hill, R. L., 1993. Surface rupture along a portion of the Emerson fault, Landers
429 earthquake of June 28, 1992, California. Geology, 46, 23–26.

430 Johnson, A.M., Fleming, R.W., Cruikshank, K. M., Martosudarmo, S. Y., Johnson, N. A., Johnson
431 K. M., Wei, W., 1997. Analecta of structures formed during the 28 June 1992 Landers-Big Bear,
432 California, earthquake sequence. U.S., Geological Survey Open-File Report 97–94, 59 p.

433 Johnson, K. M., Johnson, A. M., 2002a. Mechanical models of trishear-like folds. Journal of
434 Structural Geology, 24(2), 277-287.

435 Johnson, K. M., Johnson, A.M., 2002b. Mechanical analysis of the geometry of forced-folds.
436 Journal of Structural Geology, 24(2), 401-410.

437 Kelson, K. I., Bray, J., Cluff, L., Harder, L., Kieffer, S., Lettis, W., Page, W., Perkins, W., Rix, G.,
438 Roblee, C., Sitar, N., Wells, D., Wright, R., Yashinsky, M., 2001. Fault-related surface
439 deformation. Earthquake Spectra, 17(S1), 19-36.

440 Lazarte, C. A., Bray, J. D., Johnson, A. M., Lemmer, R. E., 1994. Surface breakage of the 1992
441 Landers earthquake and its effects on structures. Seismological Society of America Bulletin, 84,
442 547–561.

443 Leon, L. A., Christofferson, S. A., Dolan, J. F., Shaw, J. H., Pratt, T. L., 2007. Earthquake‐by‐
444 earthquake fold growth above the Puente Hills blind thrust fault, Los Angeles, California:
445 Implications for fold kinematics and seismic hazard. Journal of Geophysical Research: Solid Earth,
446 112(B3).

447 Lin, M. L., Wang, C. P., Chen, W. S., Yang, C. N., Jeng, F.S., 2007. Inference of trishear-faulting
448 processes from deformed pregrowth and growth strata. Journal of Structural Geology, 29(7), 1267-
449 1280.

Lin, M. L., Chung, C. F., Jeng, F. S., 2006. Deformation of overburden soil induced by thrust fault slip. Engineering Geology, 88(1-2), 70-89.

Livio, F. A., Michetti, A. M., Sileo, G., Zerboni, A., Trombino, L., Cremaschi, M., Mueller, K., Vittori, E., Carcano, C., Rogledi, S., 2009. Active fault-related folding in the epicentral area of the December 25, 1222 (Io= IX MCS) Brescia earthquake (Northern Italy): seismotectonic implications. Tectonophysics, 476(1), 320-335.

Livio, F. A., Berlusconi A., Zerboni A., Trombino L., Sileo, G. Michetti, A. M., Rodnight, H., Spötl, C. 2014. Progressive offset and surface deformation along a seismogenic blind thrust in the Po Plain foredeep (Southern Alps, Northern Italy). Journal of Geophysical Research: Solid Earth, 119(10), 7701-7721.

Livio, F., Michetti, A. M., Vittori, E., Gregory, L., Wedmore, L., Piccardi, L., Tondi, E., Roberts, G., Blumetti, A.M., Bonadeo, L., Brunamonte, F., Comerci, V., Di Manna, P., Ferrario, M.F., Faure Walker, J., Frigerio, C., Fumanti, F., Guerrieri, L., Iezzi, F., Leoni, G., McCaffrey, K., Mildon, Z., Phillips, R., Rhodes, E., Walters, R.J., Wilkinson, M., 2016. Surface faulting during the August 24, 2016, central Italy earthquake (Mw 6.0): preliminary results. Annals of Geophysics, 59 (Fast Track 5), 1-8.

Marchetti, M., 1996. Variazioni idrodinamiche dei corsi d'acqua della Pianura Padana centrale connesse con la deglaciazione. Il Quaternario, 9, 465–472.

Mitra, S., Mount, V. S., 1998. Foreland basement-involved structures. American Association of Petroleum Geologists Bulletin, 82, 70-109.

Moss, R. E. S., Buelna, M., Stanton, K.V., 2018. Physical, Analytical, and Numerical Modeling of Reverse Fault Displacement through Near Surface Soils. Bulletin of the Seismological Society of America, 108(6), 3149-3159.

473 Moss, R. E. S., Ross, Z. E., 2011. Probabilistic fault displacement hazard analysis for reverse
474 faults. Bulletin of the Seismological Society of America, 101(4), 1542-1553.

475 Moss, R. E. S., Stanton, K.V., Buelna, M.I., 2013. The impact of material stiffness on the likelihood
476 of fault rupture propagating to the ground surface. Seismological Research Letters, 84(3), 485-488.

477 Narr, W., Suppe, J., 1994. Kinematics of basement-involved compressive structures. American
478 Journal of Science, 294, 802-860.

479 Pucci, S., De Martini, P. M., Civico, R., Villani, F., Nappi, R., Ricci, T., Azzaro, R., Brunori, C.A.,
480 Caciagli, M., Cinti, F. R., Sapia, V., De Ritis, R., Mazzarini, F., Tarquini, S., Gaudiosi, G., Nave,
481 R., Alessio, G., Smedile, A., Alfonsi, L., Cucci, L., Pantosti, D., 2017. Coseismic ruptures of the 24
482 August 2016, Mw 6.0 Amatrice earthquake (central Italy). Geophysical Research Letters, 44(5),
483 2138-2147.

484 Quigley, M. C., Hughes, M. W., Bradley, B. A., van Ballegooy, S., Reid, C., Morgenroth, J.,
485 Horton, T., Duffy, B., Pettinga, J. R., 2016. The 2010–2011 Canterbury earthquake sequence:
486 Environmental effects, seismic triggering thresholds and geologic legacy. Tectonophysics, 672,
487 228-274.

488 Quigley, M., Van Dissen, R., Litchfield, N., Villamor, P., Duffy, B., Barrell, D., Furlong, K., Stahl,
489 T., Bilderback, E., Noble, D., 2012. Surface rupture during the 2010 Mw 7.1 Darfield (Canterbury)
490 earthquake: Implications for fault rupture dynamics and seismic-hazard analysis. Geology, 40, 55–
491 58, doi:10.1130/G32528.1.

492 Roche, V., Homberg, C., Rocher, M., 2013. Fault nucleation, restriction, and aspect ratio in layered
493 sections: quantification of the strength and stiffness roles using numerical modeling. Journal of
494 Geophysical Research: Solid Earth, 118(8), 4446-4460.

Roering, J. J., Cooke, M. L., Pollard, D.D., 1997. Why blind thrust faults do not propagate to the Earth's surface: Numerical modeling of coseismic deformation associated with thrust‐related anticlines. Journal of Geophysical Research: Solid Earth, 102(B6), 11901-11912.

Schlische, R. W., Withjack, M. O., Eisenstadt, G., 2002. An experimental study of the secondary deformation produced by oblique-slip normal faulting. American Association of Petroleum Geologists Bulletin, 86, 885–906.

Shirahama, Y., Yoshimi, M., Awata, Y., Maruyama, T., Azuma, T., Miyashita, Y., Mori, H., Imanishi, K., Takeda, N., Ochi, T., Otsubo, M., Asahina, D., Miyakawa, A., 2016. Characteristics of the surface ruptures associated with the 2016 Kumamoto earthquake sequence, central Kyushu, Japan. Earth, Planets and Space, 68(1), 191.

SM Working Group, 2015. Guidelines for Seismic Microzonation, Conference of Regions and Autonomous Provinces of Italy, Civil Protection Department, English edition of: Gruppo di lavoro MS, Indirizzi e criteri per la microzonazione sismica, Conferenza delle Regioni e delle Province autonome – Dipartimento della protezione civile, Roma, 2008, 3 vol. e Dvd, 2015. Available online at http://www.protezionecivile.gov.it/httpdocs/cms/attach_extra/GuidelinesForSeismicMicrozonation.pdf

Teran, O. J., Fletcher, J. M., Oskin, M. E., Rockwell, T. K., Hudnut, K. W., Spelz, R. M., Akciz, S., Hernandez-Flores, A.P., Morelan, A., 2015. Geologic and structural controls on rupture zone fabric: A field-based study of the 2010 Mw 7.2 El Mayor–Cucapah earthquake surface rupture. Geosphere, 11(3), 899-920.

Technical Commission for Seismic Microzonation, 2015. Linee guida per la gestione del territorio in aree interessate da Faglie Attive e Capaci (FAC), versione 1.0. Conferenza delle Regioni e delle Province Autonome – Dipartimento della Protezione Civile, 55 pp., Roma, 2015 (In Italian).

517 Tchalenko, J. S., 1970. Similarities between shear zones of different magnitudes. Geological
518 Society of America Bulletin, 81, 1625–1640, doi:10.1130/0016-7606(1970)81[1625:SBSZOD ]2.0
519 .CO;2.

520 Tchalenko, J. S., Ambraseys, N. N., 1970. Structural analysis of the Dasht-e Bayaz (Iran)
521 earthquake fractures. Geological Society of America Bulletin, 81, 41–60, doi:10.1130/0016-
522 7606(1970)81[41:SAOTDB]2.0.CO;2.

523 Thebian, L., Najjar, S., Sadek, S., Mabsout, M., 2018. Numerical investigation of dip-slip fault
524 propagation effects on offshore seabed sediments. Engineering Geology, 237, 149-167.

525 Treiman, J. A., 2010. Fault Rupture and Surface Deformation: Defining the Hazard. Environmental
526 & Engineering Geoscience, 16(1), 19-30.

527 Williams, G., Chapman, T., 1983. Strains developed in the hangingwalls of thrusts due to their
528 slip/propagation rate; a dislocation model. Journal of Structural Geology, 5(6), 563-571.

529 Youngs, R. R., Arabasz, W. J., Anderson, R. E., Ramelli, A. E., Ake, J. P., Slemmons, D. B.,
530 McCalpin., J., Doser, D. I., Fridrich, C. J., Swan, F. H., Rogers, A. M., Yount, J. C., Anderson, L.
531 W., Smith, K. D., Bruhn, R. L., Knuepfer, P.L.K., Smith, R. B., dePolo, C. M., O'Leary, D. W.,
532 Coppersmith, K.J., Pezzopane, S.K., Schwartz, D.P., Whitney, W., Olig, S.S., Toro, G.R., 2003. A
533 methodology for probabilistic fault displacement hazard analysis (PFDHA). Earth Spectra 19, 191–
534 219.

535 Zehnder, A. T., Allmendinger, R. W., 2000. Velocity field for the trishear model. Journal of
536 Structural Geology, 22(8), 1009-1014.

537 Zerboni, A., Trombino L., Frigerio, C., Livio, F., Berlusconi, A., Michetti, A. M., Rodnight, H.,
538 Spötl, C., 2015. The loess-paleosol sequence at Monte Netto: a record of climate change in the
539 Upper Pleistocene of the central Po Plain, northern Italy. Journal of Soils and Sediments, 15(6),
540 1329-1350.

541 Zinke, R., Hollingsworth, J., Dolan, J. F., 2014. Surface slip and off-fault deformation patterns in
542 the 2013 Mw 7.7 Balochistan, Pakistan earthquake: Implications for controls on the distribution of
543 near-surface coseismic slip. Geochemistry, Geophysics, Geosystems, 15(12), 5034-5050.